Broad luminescence of Ce^{3+} in multiple sites in $(La,Ce,Y)_6Si_4S_{17}$

Yasushi Nanai[1], Hayato Kamioka[2] and Tsuyoshi Okuno[3]

[1] Department of Electrical Engineering and Electronics, Aoyama Gakuin University, Sagamihara, Kanagawa 252-5258, Japan

[2] Department of Physics, Nihon University, Setagaya, Tokyo 156-8550, Japan

[3] Department of Engineering Science, The University of Electro-Communications, Chofu, Tokyo 182-8585, Japan

E-mail: `nanai@ee.aoyama.ac.jp`

Abstract. We have developed novel broad luminescent phosphors $(La,Ce,Y)_6Si_4S_{17}$ including multiple substituted sites of Ce^{3+}. They have been formed a triclinic structure (P-1) with three kinds of coordination structures around Ce^{3+} ions. The broad photoluminescence (PL) spectra at the range from 430 nm to 700 nm were observed, and they can be respectively decomposed into three PL bands. Moreover, the correlation between the three PL bands and the three substitution sites for Ce^{3+} were confirmed through the PL spectra at 78 K and a Van Uitert's universal equation.

1. Introduction

Along with the development of GaN-based light-emitting diodes (LED) [1, 2], white LEDs have attracted much interest as energy-saving, reliable and environmentally friendly light sources. Commercial white LED consists of a blue-LED and one or more phosphor materials, and is usually called phosphor converted LED (pc-LED). The phosphor materials partially convert the blue-LED emission. Ce^{3+}, Eu^{2+} and Mn^{2+} ions are well used as the activator for such broad luminescent phosphors. Because the emission band width can be expanded to some extent through the applied crystal field in hosts. The typical phosphor is a YAG:Ce^{3+}-based yellow phosphor [3, 4, 5]. However, this phosphor has less red fluorescence. So it exhibits low color rendering index and high correlated color temperature. To improve the color characteristics for better lighting systems, the phosphors having wide emission bandwidth are required. Recently, oxide, sulfide, nitride and oxy-nitride phosphors have been reported as candidates for such the phosphors. They are classified into the following two types.

The first group of phosphor contains multiple activator ions in a host [6, 7, 8, 9]. They have several luminescence peaks originating from 4f-5d transition (Ce^{3+} or Eu^{2+}) or 3d-3d transition (Mn^{2+}). For example, $Y_{10}(Si_6O_{22}N_2)O_2$:Ce^{3+},Mn^{2+} shows wide luminescence ranging from 350 nm to 700 nm, originating from $5d^1 \rightarrow 4f^1$ transition of Ce^{3+} and $^4T_1(^4G) \rightarrow {}^6A_1(^6S)$ transition of Mn^{2+} [6].

The second group phosphor contains a single activator ion in the host having multiple substitution sites [10, 11, 12, 13, 14]. $Y_3Si_5N_9O$:Ce^{3+} phosphor, a representative example, has two different substituted sites of Ce^{3+} [13]. This shows a broad luminescent band covering from blue to deep red light (450-850 nm) with the internal quantum efficiency (17.2%). A disappointing feature of this phosphor is that it requires high temperatures and reducing atmosphere to produce. On the other hand, thiosilicate phosphors also have multiple substitution sites and can be fabricated at relatively low temperature [15, 16, 17, 18, 19, 20, 21]. Especially, we have confirmed that the monoclinic $(Gd,Ce)_4(SiS_4)_3$ and $(Y,Ce)_4(SiS_4)_3$ show broad luminescence originated from Ce^{3+} ions replaced with the multiple Y or Gd sites in $Y_4(SiS_4)_3$ and $Gd_4(SiS_4)_3$ [20]. They have high internal quantum efficiency (62%) and host excitation efficiency, and also high water-resistance. The superior luminescence properties and the water-resistance depend on the host materials. However, there is no report other efficient phosphors using rare-earth thiosilicate hosts.

There are many rare-earth thiosilicate crystals. The fabrication processes have been reported for monoclinic $Ln_4(SiS_4)_3$ (Ln = Gd, Tb or Dy) [22, 23, 24], Ln_2SiS_5 (Ln = La, Ce) [25, 26], Eu_2SiS_4 [27], $EuSi_2S_5$ [18], hexagonal $Ln_6Si_{2.5}S_{14}$ (Ln = Y, Gd, Tb or Dy) [28], trigonal $Ln_4Si_3S_{12}$ (Ln = Ce, Pr, Nd, Sm or Gd) [26, 29] and triclinic $Ln_6Si_4S_{17}$ (Ln = Ce, Pr, Nd or Sm) [26, 30].

The triclinic thiosilicate crystals have distinct six rare-earth sites, categorized into three kinds of coordination structures around rare-earth ions. A triclinic phosphor $Ce_6Si_4S_{17}$ (space group P-1) exhibits much broad luminescence at the range from 443 nm

to 668 nm. In addition, it have been confirmed from differential thermal analysis and thermogravimetry analysis that this has a good thermal stability up to 500°C [26]. However, the internal quantum efficiency is quite low (10%) due to concentration quenching of Ce^{3+}. If the quenching can be eliminated, Ce^{3+}-doped triclinic rare-earth thiosilicates will be promising broad luminescent and high efficiency phosphors. A possible solution is to replace most of the six sites with different ions.

In this paper, we report novel broad luminescent phosphors $(La_{0.9-x}Ce_xY_{0.1})_6Si_4S_{17}$ ($0 \leq x \leq 0.2$). These were prepared by replacing the most sites of Ce with La or Y in $Ce_6Si_4S_{17}$ and maintaining a triclinic structure (P-1). The photoluminescence (PL) spectra were observed from blue to red region, originating from the electron transition from $5d^1$ excited state to $4f^1$ (^2F_J, $J = 5/2, 7/2$) ground state in Ce^{3+} ions. The photoluminescence excitation (PLE) spectra were broadened with increase of Ce concentration. It was found from the PL measurements at low temperature that three different PL and PLE bands are included in the spectra. Here, we discuss the correlation between the PL bands and the substitution sites of Ce^{3+} in $La_6Si_4S_{17}$.

2. Experimental Procedure

For the fabrication of polycrystalline $(La_{0.9-x}Ce_xY_{0.1})_6Si_4S_{17}$ powders, we used the solid state reaction technique in vacuum-sealed silica-glass ampoule. A mixture of La_2S_3, Ce_2S_3, Y_2S_3, Si and S powders in the molar ratio of $La_2S_3 : Ce_2S_3 : Y_2S_3 : Si : S = 3(0.9 - x) : 3x : 0.3 : 4.4 : 8.8$ was prepared. The total weight of the powder was ∼300 mg. The value x refers to Ce concentration in the range of 0-0.2. To obtain the single phase triclinic $(La_{0.9-x}Ce_xY_{0.1})_6Si_4S_{17}$ phosphors, additional Y_2S_3 was needed. When the phosphors were fabricated without the addition, monoclinic La_2SiS_5 phase was appeared in them (experimental data are not shown here). To avoid a residual of rare-earth sulfide after thermal heating, a 10% molar excess of Si and S were added in the starting mixture. The mixture was sealed in a silica-glass ampoule in a vacuum of 10^{-2} Pa. For the first annealing, the ampoule was heated for 24 h at 1050°C. Since a trace of other phase still existed in the powders after the annealing, the powders and additional sulfur (20 mg) were milled and heated again for 24 h at 1050°C after sealing in a vacuum silica tube.

X-ray diffraction (XRD) patterns were recorded using a Rigaku Rint2000 diffractometer in standard θ-2θ geometry using Cu K_α radiation. Structural information such as lattice constants was obtained through the Rietveld method. The atomic positions and thermal expansion factors were not refined, because they require higher quality XRD patterns.

The third harmonic of a pulsed Nd:YAG laser (355 nm, 10 kHz) and monochromatic output from a xenon arc lamp were used as the excitation source for PL measurements. The latter was also used for PLE measurements. A charge-coupled device camera and a photomultiplier were used for photo-detection in the PL and PLE measurements. The second harmonic of a pulsed Ti:sapphire laser (400∼440 nm, 82 MHz, pulse duration <

130 fs) and a spectrometer with a streak camera (Hamamatsu-Photonics C5680) were used for time-resolved PL measurements. An excitation pulse was picked up by using a Pockels cell. The system time resolution was 0.8 ns. These measurements were carried out with a cryostat in a temperature range of 78-300 K. Internal quantum efficiency was measured using a spectrophotometer (Hamamatsu C11347-01) having an integrating sphere. Sample powder (∼20 mg) was put on a quartz Petri dish which was placed within the integrating sphere. Monochromatic output from 300 nm to 500 nm of a xenon arc lamp was used for the excitation. Details of the measurement can be found in [18].

3. Results and discussion

3.1. XRD results

Figure 1 shows XRD patterns of $(La_{0.9-x}Ce_xY_{0.1})_6Si_4S_{17}$ (x = 0-0.2). In the top of this figure, a simulated XRD pattern for $Ce_6Si_4S_{17}$ is placed. The simulation was conducted using the crystallographic data of $Ce_6Si_4S_{17}$ [26] and the RIETAN-FP program [31]. Line shapes were models by pseudo-Voigt profile functions. For the all of samples, the XRD pattern are well understood only shifts from that of $Ce_6Si_4S_{17}$, and no peak for starting materials and no unidentified peak were confirmed. This indicates that single phase triclinic $(La_{0.89-x}Ce_xY_{0.1})_6Si_4S_{17}$ powders were obtained in this work. Ce^{3+} and Y^{3+} ions would be substituted for La sites in $La_6Si_4S_{17}$ hosts. At present, the triclinic-type lanthanum thiosilicate has not been reported. From the diffraction peak positions of the XRD pattern for $(La_{0.9}Y_{0.1})_6Si_4S_{17}$, the lattice constants were estimated at $a = 8.99$ Å, $b = 10.02$ Å, $c = 14.28$ Å, $\alpha = 82.21°$, $\beta = 86.96°$, $\gamma = 89.47°$, respectively. With the increase in x, the lattice constants a, b and c are decreased. For example, the lattice constants of $(La_{0.7}Ce_{0.2}Y_{0.1})_6Si_4S_{17}$ were estimated at $a = 8.98$ Å, $b = 10.01$ Å, $c = 14.27$ Å, $\alpha = 82.22°$, $\beta = 86.96°$, $\gamma = 89.45°$, respectively. This can be understood as arising from the substitution of La^{3+} by Ce^{3+}, since the ionic radius of Ce^{3+} is 2% smaller than that of La^{3+} [32]. It can be also understood that the lattice constants a, b and c of $(La_{0.9}Y_{0.1})_6Si_4S_{17}$ are 0.3%, 0.2% and 0.1% larger than that of $Ce_6Si_4S_{17}$, respectively, considering their ionic radii.

3.2. Photoluminescence at room temperature

Figure 2 shows PL spectra and PLE spectra of $(La_{0.9-x}Ce_xY_{0.1})_6Si_4S_{17}$. This broad PL band from 420 nm to 720 nm originates from $5d^1 \rightarrow 4f^1$ (^2F_J, $J = 5/2, 7/2$) transition of Ce^{3+} replaced with La sites in the hosts. With the increase in x, the PL peak slightly shifts from 532 nm to 536 nm, while the full width at half maximum (FWHM) of the PL band decreases from 107 nm to 97 nm. The maximum internal quantum efficiency was found to be 59% for $x = 0.07$, and kept after immersion in distilled-water for a day at room temperature (details on the measurement can be found in [20]). It could be confirmed that the phosphors also have high water resistance, same as $(Gd,Ce)_4(SiS_4)_3$

and $(Y,Ce)_4(SiS_4)_3$ [20]. For the PLE band, the FWHM significantly increases from 70 nm to 129 nm with the increase in x. The complicated dependence of PL and PLE spectra on Ce concentration can be explained by the multiple substitution sites of Ce^{3+} in $(La_{0.9-x}Ce_xY_{0.1})_6Si_4S_{17}$. The atomic positions of $La_6Si_4S_{17}$ have not yet been refined by the XRD patterns. Thus, we discuss the S^{2-} coordination structures around rare-earth ions in $La_6Si_4S_{17}$ with reference to those of $Ce_6Si_4S_{17}$ having similar triclinic structure.

The Ce-S coordination structures around each Ce sites in $Ce_6Si_4S_{17}$ are summarized in table 1. The volume (V_c) of the Ce-S coordination structure and the average distance (R_a) between Ce and S were estimated by VESTA [33]. $Ce_6Si_4S_{17}$ has distinct six Ce sites, and they are mainly classified into three types according to their coordination structure and number. The schematic of the three coordination structures, mono-capped trigonal prism (1ctp), bi-capped trigonal prism (2ctp) and tri-capped trigonal prism (3ctp), are shown in figure 3. There are one 1ctp, three 2ctp and two 3ctp in $Ce_6Si_4S_{17}$. The Ce sites belonging to the same prism group have almost the same V_c and R_a. $La_6Si_4S_{17}$ has also six distinct La sites similar to $Ce_6Si_4S_{17}$. The 4f-5d transitions in Ce^{3+} related to the PL and PLE bands depend on the coordination environment around the ion, which causes the 5d level splitting through crystal field. Therefore, it can be assumed that the PL and PLE spectra of $(La_{0.9-x}Ce_xY_{0.1})_6Si_4S_{17}$ contain three types of PL and PLE bands, which are related to the three prism structures. In the next subsection, we will discuss the validity of this assumption through fine analysis of the spectra measured at 78 K.

3.3. Photoluminescence at low temperature (at 78 K)

Figure 4 shows excitation wavelength ($\lambda_{ex.}$) dependence of PL spectra for $(La_{0.9-x}Ce_xY_{0.1})_6Si_4S_{17}$ (x = 0.01 (a) and 0.2 (b)) at 78 K. They have a few peaks commonly and their spectral shapes were changed dramatically as the excitation wavelength was shifted from 410 nm to 480 nm. These indicate that the PL spectrum includes several intrinsic PL bands. The PL spectrum from Ce^{3+} in a La site consists two bands, corresponding to the transitions from $5d^1$ to $^2F_{7/2}$ and $^2F_{5/2}$ levels in the $4f^1$ configuration, respectively. The energy level of $^2F_{7/2}$ is higher than that of $^2F_{5/2}$, so the PL band for the former is placed at longer wavelength side. From now on, we will treat the two PL bands originating from Ce^{3+} in a La site as one unit. At first, we discuss the PL spectra shown in figure 4 (a). The spectrum for 480 nm excitation clearly shows simple double peaks, so this can be ascribed to Ce^{3+} ions in a La site. We termed the PL unit "X1" band. As for the excitation at 440 nm, the PL spectrum shifts to lower wavelength and has a tail on the long wavelength side. This indicates that an additional PL unit, ascribed to the Ce^{3+} ions in another kind of La site, was excited. Here we named this as "X2" band. The spectrum for the excitation at 410 nm also showed the shift and long tail. These can be interpreted in the same way. That is, a third PL unit was excited. The last one can be termed as "X3" band, corresponding

to Ce^{3+} in a third kind of La site. In figure 4(b) for $x = 0.2$, the PL peak located at 460 nm was not observed even when excited at 410 nm. This might be due to the concentration quenching of Ce^{3+} related to X3 band, and will be discussed in the next measurement of PL decay curves. The spectra for 440 and 480 nm excitation had no change from those of $x = 0.01$. The result indicates that X1 and X2 bands would not shift with increasing Ce concentration. Thus, it is considered that the spectral change, varying with the excitation wavelength as shown in figure 2 and figure 4, is due to the intensity ratio of the X1, X2 and X3 bands.

Detection wavelength dependence of PLE spectra for $(La_{0.89}Ce_{0.01}Y_{0.1})_6Si_4S_{17}$ at 78 K is shown in figure 5. The PLE peaks in the long wavelength region are located at 410, 440 and 475 nm for the PL detection at 460, 500 and 620 nm, respectively. They would originate from the $4f^1(^2F_{5/2}) \rightarrow 5d^1$ transition for Ce^{3+} in three different La sites. The excitation wavelengths used for the PL measurement in figure 4 were located near these peaks. Thus, it can be assumed that the discussion about PL spectra in figure 4 is plausible. That is, the observed PLE peaks at 475, 440 and 410 nm are the origins of the X1, X2 and X3 PL bands, respectively.

To assign the X1, X2 and X3 bands, we demonstrated fitting the PL spectra shown in figure 4(a) using Gaussian curves. Figure 6(a), (b) and (c) show the fitting result for the PL spectrum, shown in figure 4(a), excited at 480, 440 and 410 nm, respectively. Here, the PL spectra are represented by open circles and the fitting results are shown by solid lines. The bottom axis was changed to the photon energy for the fitting. Firstly, it is found that the PL spectrum in figure 6(a), having narrow two peaks, could be fitted by just two Gaussian curves, as represented by a dashed-dotted line. This indicates that the PL spectrum induces from the X1 band, belonging to the lowest energy site. Secondly, the PL spectrum in figure 6(b), showing blue shift and broadening of the spectral shape, could be clearly represented by the two curves and additional two Gaussians. In this fitting, we fixed the peak widths, positions and intensity ratios between these two peak intensities of the former, corresponding to the X1 band. The additional two curves, as represented by a dashed line, would be assigned to the X2 band. Finally, the PL spectrum in figure 6(c) could be also reproduced by the same manner. Before the fitting, we fixed the peak widths, positions and intensity ratios between these two peak intensities for the X1 and X2 bands. Then the spectrum was well fitted with additional two Gaussians. The additional two, as represented by a dotted line, could be assigned to the X3 band. The obtained parameters, peak positions and their energy differences, are summarized in table 2. As mentioned before, the lower side peak in the curve pairs corresponds to the transition from $5d^1$ to $4f^1(^2F_{7/2})$, while the higher comes from $5d^1$ to $4f^1(^2F_{5/2})$ transition. The energy differences, corresponding to the spin-orbit splitting of the $4f^1$ level in Ce^{3+} ion, are similar with that for $(Gd,Ce)_4(SiS_4)_3$ (0.24 eV) and $(Y,Ce)_4(SiS_4)_3$ (0.24 eV) [20]. This indicates that our deconvolution process is adequate for the analysis of the emission bands in $(La_{0.89}Ce_{0.01}Y_{0.1})_6Si_4S_{17}$.

In the previous paragraph, the PL spectrum of $(La_{0.89}Ce_{0.01}Y_{0.1})_6Si_4S_{17}$ could be divided into three PL bands. However, the PL bands have not yet been associated with

the each specific La sites. To clarify the correspondence between the three PL bands and the three kinds of Ce ions substituted for La sites in $La_6Si_4S_{17}$, we discussed with the following empirical equation [34].

$$E/Q = \left[1 - (V/4)^{1/V} 10^{-(nrA/80)}\right], \tag{1}$$

where E is the lowest emission or excitation energy of a Lanthanide ion taken in a host crystal, and Q is the d-band energy when the ion is in free space. V is the valence of the ion. A is the electron affinity of a ligand anion. n is the coordination number around the ion. r is the ionic radius of a host cation substituted by the ion. This formula gives the correspondence between the emission energy and the anion coordination around the host cation in the first approximation. What matters in this correspondence is not details of the coordination structure but the type and number of anions and the ionic radius of host cations. Van Uitert have succeeded in explaining the emission peak and/or excitation edge energies for Eu^{2+} or Ce^{3+} systematically by using this equation in many hosts such as sulfide, oxide, halide and aluminates [34]. In this report, we attempt to relate the three PL bands to the three coordination structures, based on the equation. Here, the peak energies of $5d^1 \rightarrow 4f^1$ ($^2F_{5/2}$) transition in table 2 were substituted in E. The units of the peak energies were changed to wavenumber. The Q value is 50,000 cm^{-1} and $V = 3$ for Ce^{3+}. According to Van Uitert, the A value is uniformly constant in the same host materials. Thus, it is assumed that A of S^{2-} anions in $La_6Si_4S_{17}$ is also constant. However, it is difficult to estimate A for sulfur in $(La_{0.9-x}Ce_xY_{0.1})_6Si_4S_{17}$ from other experiments. The ionic radius r of the La ion increases with increasing n [32]. Hence, the value of E/Q for the PL band in $(La_{0.89}Ce_{0.01}Y_{0.1})_6Si_4S_{17}$ increase with the coordination number of the La site. According to table 1 and 2, X1, X2 and X3 bands should correspond to 1ctp, 2ctp and 3ctp structures of the La sites, respectively.

Figure 7 depicts E/Q versus $(nrA)/80$ for $(La_{0.89}Ce_{0.01}Y_{0.1})_6Si_4S_{17}$ and other rare-earth thiosilicate phosphors. The data and references for them are summarized in table 3. The solid curve represents equation (1) for Ce^{3+} ($V = 3$). The A value was estimated as 1.56 eV by least squares fitting for the data of $(La_{0.89}Ce_{0.01}Y_{0.1})_6Si_4S_{17}$. To check the validity of this estimation, the corresponding data for $(Gd_{0.99}Ce_{0.01})_4(SiS_4)_3$ and $(Y_{0.99}Ce_{0.01})_4(SiS_4)_3$ with the same A value were plotted in this figure. All the points lines up on the solid curve with good accuracy. Van Uitert described that the A values for oxy-anion complexes involving the highly charged central cations, such as SiO_4^{4-}, PO_4^{3-} and WO_4^{4-}, were generally greater than those of CaO, $Y_3Al_5O_{12}$ and $Gd_3Al_5O_{12}$ without such cations [34]. Thus, it is assumed that sulfide hosts have also the same tendency. Because the A value for binary sulfide hosts, such as CaS, ZnS and La_2S_3, is 1.0 [34], the thiosilicates with SiS_4^{4-} anion, which is also highly charged complex, should have larger A value. This indicates that the estimated value of 1.56 is reasonable as the effective electron affinity of such the thiosilicate hosts. Thus, we conclude that the X1, X2 and X3 bands originate from the Ce^{3+} ions in 1ctp, 2ctp and 3ctp structures of the La sites, respectively.

To discuss the concentration quenching of the phosphor, we measured the PL decay

profiles of the X1, X2 and X3 bands. As shown in figure 6, the PL spectrum contains the three emission bands. When the phosphor is excited at 410 nm, the PL spectral part below 2.00 eV (620 nm) and above 2.69 eV (460 nm) consist only of X1 and X3 band, respectively. Then, the X2 band emission can be observed by monitoring the PL region above 2.48 eV (500 nm) with excitation at 2.81 eV (440 nm). Figure 8 shows the PL decay profiles of (a) X1, (b) X2 and (c) X3 bands in $(La_{0.9-x}Ce_xY_{0.1})_6Si_4S_{17}$ for $x = 0.01$, 0.03, 0.07 and 0.20, which were obtained at 78 K based on the method described above. In figure 8 (a), the excitation pulse shape is also appended. The excitation pulse is followed by a tiny pulse appeared at 10 ns. The second pulse is the residual left after the Pockels cell operation and does not affect the PL decay profiles. The PL data were calculated through integration of the spectral region above 620 nm (a), below 500 nm (b) and below 460 nm (c) at each delay time. These measurement conditions are summarized in table 4.

Their decay times were obtained through curve fitting with the following single or double exponential function.

$$I(t) = \sum_{i=1}^{N} I_i e^{t/\tau_i} + b \quad (N = 1 \text{ or } 2, \tau_1 < \tau_2). \tag{2}$$

The decay profiles of X1 and X2 band could be fitted by a single exponential regardless of the Ce concentration. The decay profile of X3 band for $x = 0.01$ sample could be also fitted by this way. However, the X3 profiles for $x = 0.03$ and 0.07 samples had to be fitted by double exponential. The X3 band was not observed for the $x = 0.20$ sample because of the concentration quenching of Ce^{3+}. The fast components (τ_1) of the decay times are summarized in figure 9. The decay time of X3 band decreased from 20.5 ns to 4.8 ns with the increase of Ce concentration, while those of X1 and X2 band did not change for any concentration samples as 33.9 ns for the X1 band and 28.5 ns for the X2 band.

To understand these results, we discuss the energy transfer among Ce^{3+} ions in $La_6Si_4S_{17}$ based on Dexter's theory [35]. The deconvolution analysis for the X1, X2 and X3 bands in figure 6 indicates that the peaks at the right end of the PLE spectrum in figure 5, 475 nm, 440 nm and 410 nm, correspond to the Ce^{3+} ions substituted for 1ctp, 2ctp and 3ctp, respectively. According to Dexter's theory, the energy transfer to neighboring ions can occur when the luminescence band of donor ion overlap the excitation band of acceptor ion [35]. As shown in figure 5 and 6, there is no spectral overlap between PL and PLE spectra originating from the Ce^{3+} in the same coordination structure. Thus, the energy transfer between Ce^{3+} ions in the same coordination structure does not occur. On the other hand, the X3 PL band has overlaps with the excitation bands for X1 and X2 band. Therefore, the energy transfer from Ce^{3+} in 3ctp sites to Ce^{3+} in 2ctp or 1ctp sites is possible. The energy transfer from Ce^{3+} in 2ctp sites to Ce^{3+} in 1ctp sites can also occur because the X2 PL band overlaps a little with the excitation band for the X1 band, while the energy transfer from Ce^{3+} in 1ctp to others are impossible.

The Dexter's theory also indicates that the probability of the energy transfer increases in proportion to R^{-6} (electric dipole-dipole interaction), where R is the distance between donor ion and acceptor ion [35]. This leads to the prospect that the energy transfer from 2ctp or 3ctp sites to 1ctp sites hardly occur even when the Ce^{3+} ions are highly doped in the host, since the number of 1ctp site is smaller than that of 2ctp or 3ctp site, as shown in table 1. On the other hand, the energy transfer from 3ctp sites to 2ctp sites increases with increase of Ce concentration because the number of those sites is comparable. That is, the energy transfer from 3ctp sites to 2ctp sites is selectively promoted when Ce^{3+} ions are highly doped in the host. This leads to the experimental results that only the decay time of the X3 band become faster when the Ce concentration is increased.

4. Conclusions

In conclusion, we introduced novel broad luminescent phosphors $(La_{0.9-x}Ce_xY_{0.1})_6Si_4S_{17}$ (x = 0-0.2). The observed broad PL spectra at the range from 430 nm to 700 nm were originated from $5d^1 \rightarrow 4f^1$ transition in Ce^{3+}. They could be excited by near-UV, violet and blue LEDs and have maximum internal quantum efficiency of 59% for $x = 0.07$. We clarified the presence of three PL bands, each consisting of two peaks, through the PL spectra at 78 K. The correlation between the PL bands and the Ce substitution sites in the matrix could be well explained with a universal formula. The three PL bands directly correspond to the three kinds of Ce^{3+} ions replaced at the characteristic La sites in $La_6Si_4S_{17}$, whose coordination number is 7, 8 or 9. These indicate that $(La_{0.9-x}Ce_xY_{0.1})_6Si_4S_{17}$ are promising broad luminescent, efficient and stable phosphors for white LED with high color rendering.

Acknowledgments

XRD patterns and PL efficiency were measured at the Center for Instrumental Analysis in the University of Electro-Communications.

References

[1] Nakamura S, Mukai T and Senoh M 1994 *Appl. Phys. Lett.* **64** 1687
[2] Hashimoto T, Wu F, Speck J S and Nakamura S 2007 *Nat. Mater.* **6** 568
[3] Haranath D, Chander H, Sharma P and Singh S 2006 *Appl. Phys. Lett.* **89** 173118
[4] Lu C-H and Jagannathan R 2002 *Appl. Phys. Lett.* **80** 3608
[5] Kasuya R, Kawano A, Isobe T, Kuma H and Katano J 2007 *Appl. Phys. Lett.* **91** 111916
[6] Geng D, Lian H, Shang M, Zhang Y and Lin J 2014 *Inorg. Chem.* **53** 2230 2239
[7] Song K, Zhang J, Liu Y, Zhang C, Jiang J, Jiang H and Qin H-B 2015 *J. Phys. Chem. C* **119** 24558
[8] Unithrattil S, Lee K H and Im W B 2014 *J. Am. Ceram. Soc.* **97** 874
[9] Bai G, Tsang M-K and Hao J 2016 *Adv. Funct. Mater.* **26** 6330
[10] Wang L, Xie R-J, Li Y, Wang X, Ma C-G, Luo D, Takeda T, Tsai Y-T, Liu R-S and Hirosaki N 2016 *Light: Science & Applications* **5** e16155
[11] Suehiro T, Hirosaki N and Xie R-J 2011 *ACS Appl. Mater. Interfaces* **3** 811
[12] Liu Y, Zhang X, Hao Z, Wang X and Zhang J 2011 *J. Mater. Chem.* **21** 6354
[13] Zhu Q-Q, Wang Le, Hirosaki N, Hao L Y, Xu X, and Xie R-J 2016 *Chem. Mater.* **28** 4829
[14] Lin H, Bai G, Yu T, Tsang M-K, Zhang Q and Hao J 2017 *Adv. Optical Mater.* **5** 1700227
[15] Nishimura M, Nanai Y, Bohda T and Okuno T 2009 *Jpn. J. Appl. Phys.* **48** 072301
[16] Sugiyama M, Nanai Y, Okada Y and Okuno T 2011 *J. Phys. D: Appl. Phys.* **44** 095404
[17] Nanai Y, Sasaki C, Sakamoto Y, Okuno T 2011 *J. Phys. D: Appl. Phys.* **44** 405402
[18] Nanai Y, Sakamoto Y and Okuno T 2012 *J. Phys. D: Appl. Phys.* **45** 265102
[19] Nanai Y, Sakamoto Y and Okuno T 2013 *Jpn. J. Appl. Phys.* **52** 04CG15
[20] Nanai Y, Suzuki K and Okuno T 2015 *Mater. Res. Express* **2** 036203
[21] Nanai Y, Suzuki K and Okuno T 2016 *J. Phys. D: Appl. Phys.* **49** 105103
[22] Hatscher S T and Urland W 2003 *J. Solid State Chem.* **172** 417
[23] Hatscher S T and Urland W 2002 *Z. Anorg. Allg. Chem.* **628** 1673
[24] Hatscher S T and Urland W 2002 *Acta Cryst. E* **58** i74
[25] Daszkiewicz M, Gulay L D, Ruda I R, Marchukc O V and Pietraszkoa A 2007 *Acta Cryst. E* **63** i197
[26] Gauthier G, Jobic S, Evain M, Koo H-J, Whangbo M-H, Fouassier C and Brec R 2003 *Chem. Mater.* **15** 828
[27] Hartenbach I and Schleid T 2002 *Z. Anorg. Allg. Chem.* **628** 1327
[28] Perez G and Duale M 1969 *C.R. Acad. Sci. Ser. C* **269** 984
[29] Michelet A, Flahaut J 1969 *C.R. Acad. Sci. Ser. C* **268** 326
[30] Gulay L D, Daszkiewicz M, Lychmanyuk O S and Pietraszko A 2008 *J. Alloys and Compounds* **453** 197
[31] Izumi F and Momma K 2007 *Solid State Phenom.* **130** 15
[32] Shannon R D 1976 *Acta Crystallogr. Sect. A* **32** 751
[33] Momma K and Izumi F 2011 *J. Appl. Crystallogr.* **44** 1272
[34] Van Uitert L G 1984 *J. Lumin.* **28** 1
[35] Dexter D L 1953 *J. Chem. Phys.* **21** 836

Tables and table captions

Table 1. Ce-S coordination structures in $Ce_6Si_4S_{17}$ [26]. The volume (V_c) and the average distance (R_a) between Ce and S of Ce-S coordination structures were estimated by VESTA [33].

Sites	Coordination structure and (number)	V_c / Å^3	R_a / Å
Ce4	1ctp (7)	36.8	2.94
Ce3	2ctp (8)	46.6	3.00
Ce5	2ctp (8)	46.5	3.00
Cr6	2ctp (8)	47.8	3.00
Ce1	3ctp (9)	55.5	3.05
Ce2	3ctp (9)	57.1	3.07

Table 2. The peak positions of the PL bands and the separation between $^4F_{5/2}$ levels and $^4F_{7/2}$ levels (ΔE).

PL band	$5d^1 \rightarrow 4f^1(^2F_{5/2})$ / eV	$5d^1 \rightarrow 4f^1(^2F_{7/2})$ / eV	ΔE / eV
X1	2.30	2.04	0.26
X2	2.47	2.23	0.24
X3	2.69	2.42	0.27

Table 3. Data for Figure 8. Host cation radii r are given from [32].

Host materials	n	r / Å	A / eV	E ($\times 10^4$) / cm^{-1}	$nrA/80$	E/Q	Ref. of E
$La_6Si_4S_{17}$	9	1.216	1.56	2.17	0.213	0.434	This work
	8	1.16	1.56	1.99	0.181	0.399	This work
	7	1.10	1.56	1.86	0.150	0.371	This work
$Ga_4(SiS_4)_3$	8	1.053	1.56	1.78	0.164	0.357	[20]
	7	1.00	1.56	1.59	0.137	0.318	[20]
$Y_4(SiS_4)_3$	8	1.019	1.56	1.83	0.159	0.366	[20]
	7	0.96	1.56	1.64	0.131	0.328	[20]

Table 4. Measurement conditions for the PL decay of X1, X2 and X3 band at 78 K.

PL band	Coordination structure	Excitation wavelength / nm	Integral region of PL spectrum at each time point
X1	1ctp	410	> 620 nm
X2	2ctp	440	< 500 nm
X3	3ctp	410	< 460 nm

Figure captions

Figure 1. XRD patterns of $(La_{0.9-x}Ce_xY_{0.1})_6Si_4S_{17}$ ($x = 0$ to 0.2). In the top panel, the simulated pattern of $Ce_6Si_4S_{17}$ and the indices of the diffraction peaks are shown.

Figure 2. Photoluminescence (PL) and photoluminescence excitation (PLE) spectra of $(La_{0.9-x}Ce_xY_{0.1})_6Si_4S_{17}$ ($x = 0.01$ to 0.2). The value of x is shown in the figure. Excitation wavelength for the PL spectra is 355 nm. Detection wavelength for PLE spectra is 535 nm.

Figure 3. Schematic of S^{2-} coordination structures around Ce^{3+} ions in $Ce_6Si_4S_{17}$ [26]. (a) mono-capped trigonal prism (1ctp). (b) bi-capped trigonal prism (2ctp) (c) tri-capped trigonal prism (3ctp).

Figure 4. Excitation wavelength dependence of PL spectra for $(La_{0.9-x}Ce_xY_{0.1})_6Si_4S_{17}$ ($x = 0.01$ (a), 0.2 (b)) at 78 K. The excitation wavelengths were 410 nm (dotted lines), 440 nm (dashed lines) and 480 nm (dashed-dotted lines).

Figure 5. Detection wavelength dependence of PLE spectra for $(La_{0.89}Ce_{0.01}Y_{0.1})_6Si_4S_{17}$ at 78 K. Detection wavelengths were 460 nm (dotted lines), 500 nm (dashed lines) and 620 nm (dashed-dotted lines). Up arrows represent the PLE peaks in the long wavelength region located at 410, 440 and 475 nm.

Figure 6. Deconvolution results of PL spectra (circles) for $(La_{0.89}Ce_{0.01}Y_{0.1})_6Si_4S_{17}$ at 78 K. The excitation wavelengths ($\lambda_{\text{exc.}}$) are shown in the figure. X1 (dashed-dotted line), X2 (dashed line) and X3 (dotted line) are PL bands originated from $5d^1 \rightarrow 4f^1$ (^2F_J, $J = 7/2, 5/2$) transition of Ce^{3+} ions replacing different La sites in $La_6Si_4S_{17}$. (a) X1, (b) X1 and X2 or (c) X1, X2 and X3 bands are included in each PL spectra. Solid lines represent sum of the PL bands.

Figure 7. E/Q versus $nrA/80$ for $(La_{0.89}Ce_{0.01}Y_{0.1})_6Si_4S_{17}$ (circles), $(Gd_{0.99}Ce_{0.01})_4(SiS_4)_3$ (squares) and $(Y_{0.99}Ce_{0.01})_4(SiS_4)_3$ (triangles). The solid curve is calculated from equation (1) with $V = 3$. Coordination numbers n of La, Gd and Y sites are denoted near the corresponding marks.

Figure 8. PL decay curves of (a) X1, (b) X2 and (c) X3 bands in $(La_{0.9-x}Ce_xY_{0.1})_6Si_4S_{17}$ for $x = 0.01$ (circles), 0.03 (squares), 0.07 (triangles) and 0.20 (rhombuses) at 78 K. Solid lines are fitted curves by single exponential functions (equation (2), $n = 1$). Dotted lines are the fitted curves by double exponential functions (equation (2), $n = 2$). The X3 band decay for $x = 0.20$ is not observed because of quenching.

Figure 9. Changes in the decay times of X1, X2 and X3 bands for $(La_{0.9-x}Ce_xY_{0.1})_6Si_4S_{17}$ with Ce concentration x at 78 K. For $x = 0.20$, that of X3 band couldn't be plotted because it was quenched.

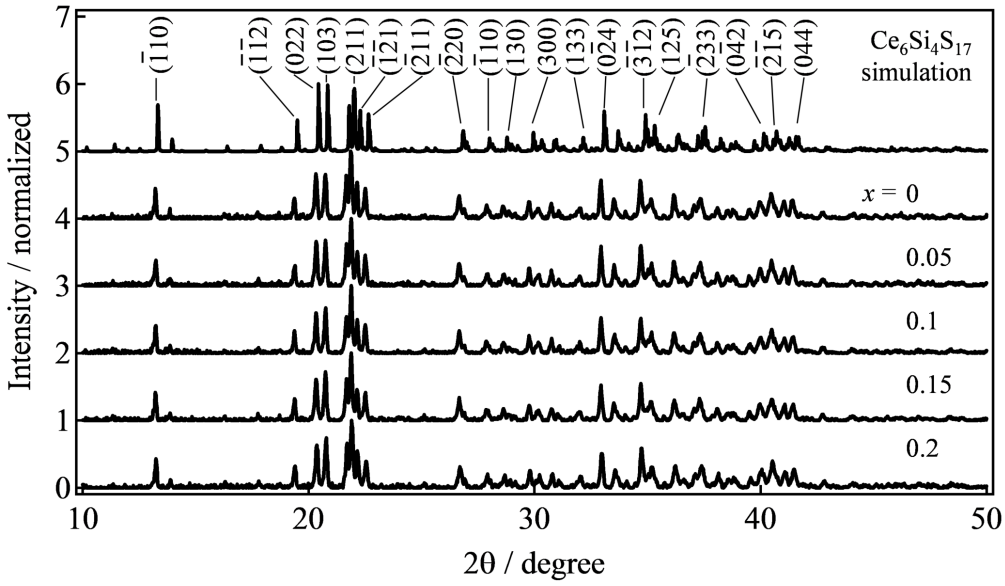
Intensity / normalized
2θ / degree
Ce6Si4S17
simulation
x = 0
0.05
0.1
0.15
0.2
(1̄10)
(1̄1̄2)
(022)
(103)
(211)
(1̄21)
(1̄11)
(220)
(1̄10)
(130)
(300)
(13̄3)
(02̄4)
(3̄12)
(125)
(1̄33)
(042)
(2̄15)
(044)

Figure 1.

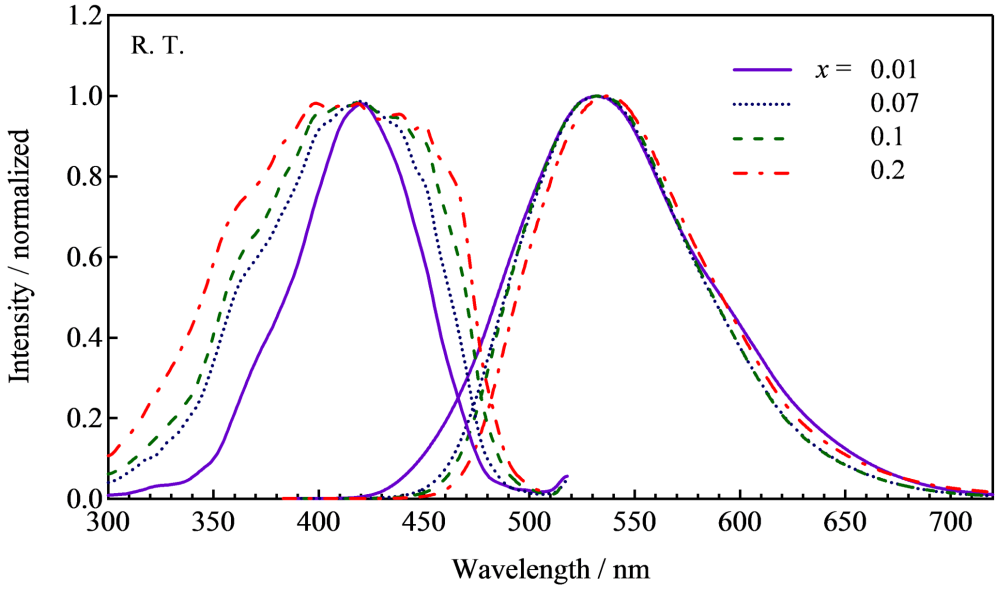
R. T.
x = 0.01
0.07
0.1
0.2
Intensity / normalized
Wavelength / nm
0.0
0.2
0.4
0.6
0.8
1.0
1.2
300
350
400
450
500
550
600
650
700

Figure 2.

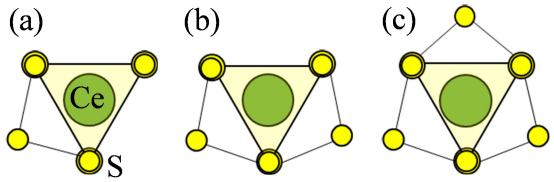

Figure 3.

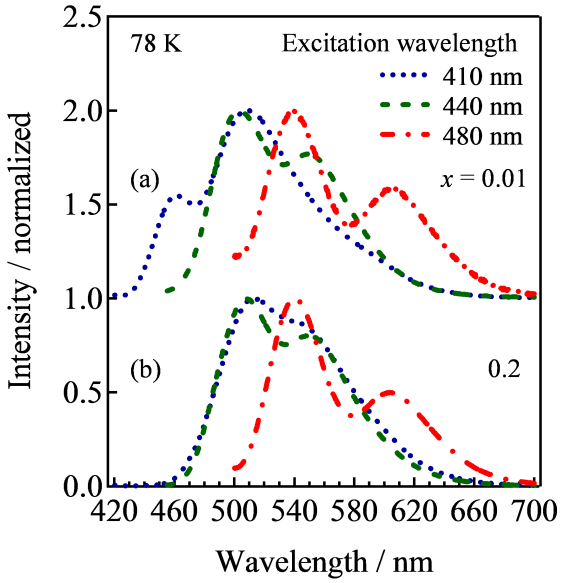
78 K
Excitation wavelength
410 nm
440 nm
480 nm
x = 0.01
(a)
(b)
0.2
Intensity / normalized
Wavelength / nm
2.5
2.0
1.5
1.0
0.5
0.0
420 460 500 540 580 620 660 700

Figure 4.

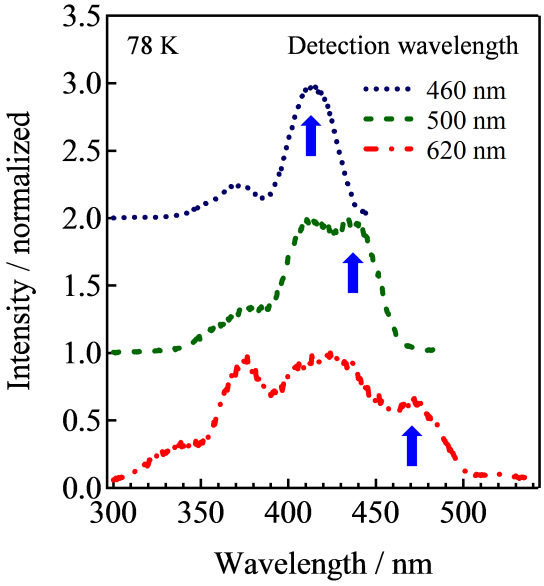
78 K
Detection wavelength
460 nm
500 nm
620 nm
Intensity / normalized
Wavelength / nm
0.0
0.5
1.0
1.5
2.0
2.5
3.0
3.5
300
350
400
450
500

Figure 5.

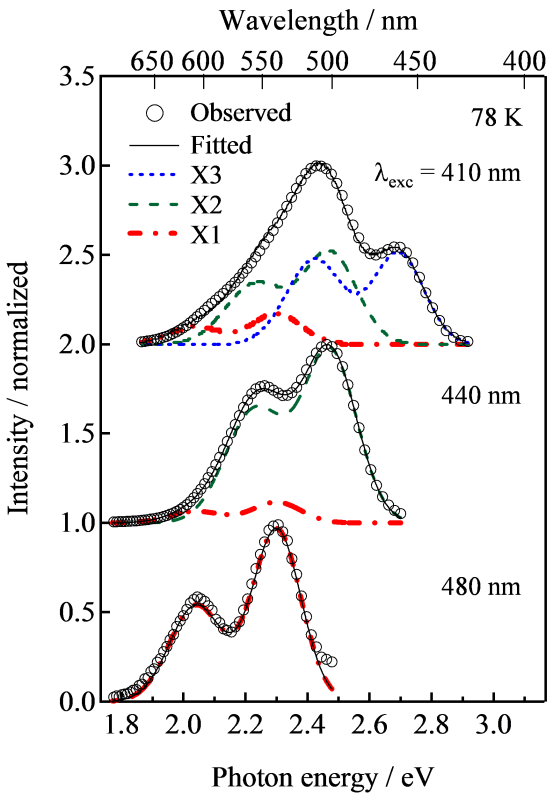
Wavelength / nm
650 600 550 500 450 400
Observed
Fitted
X3
X2
X1
78 K
λexc = 410 nm
440 nm
480 nm
Intensity / normalized
3.5
3.0
2.5
2.0
1.5
1.0
0.5
0.0
1.8 2.0 2.2 2.4 2.6 2.8 3.0
Photon energy / eV

Figure 6.

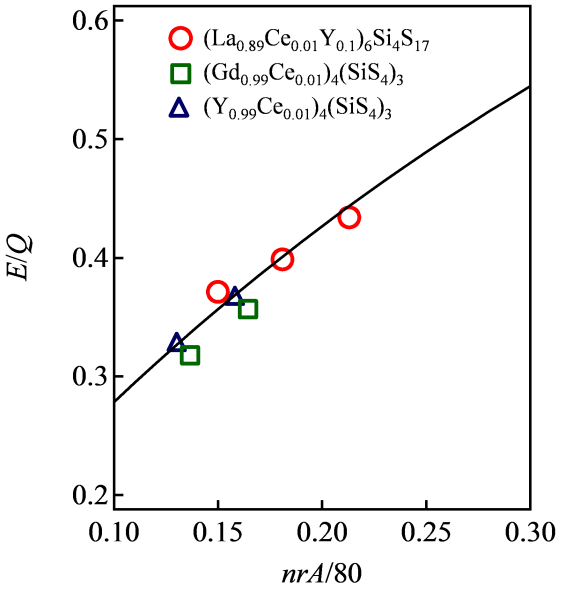
0.6
0.5
0.4
0.3
0.2
E/Q
0.10
0.15
0.20
0.25
0.30
nrA/80
(La0.89Ce0.01Y0.1)6Si4S17
(Gd0.99Ce0.01)4(SiS4)3
(Y0.99Ce0.01)4(SiS4)3

Figure 7.

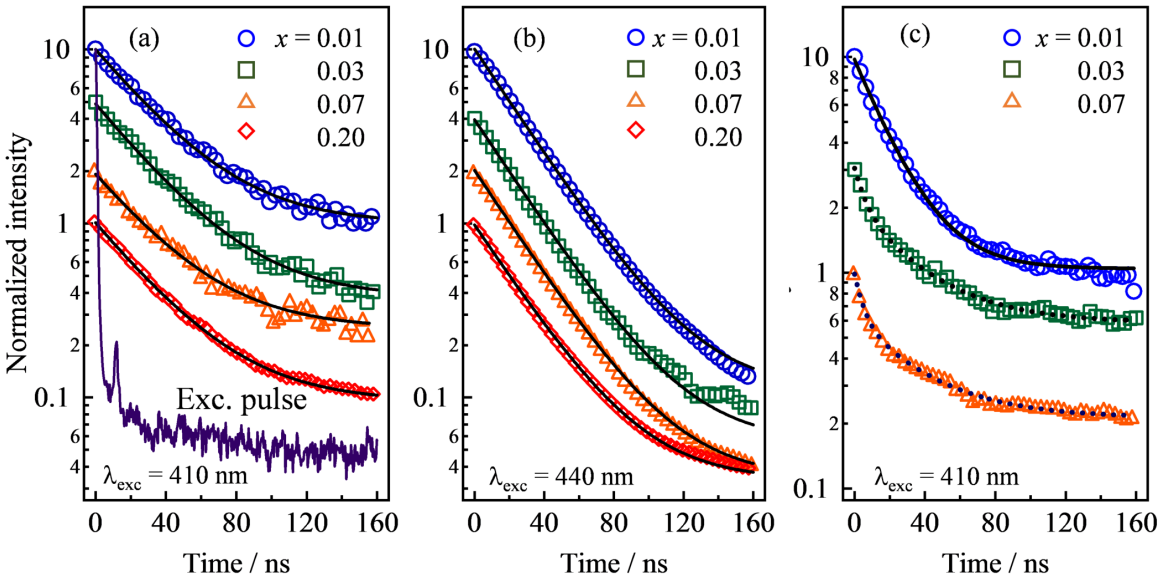
(a)
(b)
(c)
x = 0.01
0.03
0.07
0.20
Normalized intensity
Exc. pulse
λexc = 410 nm
λexc = 440 nm
λexc = 410 nm
Time / ns
Time / ns
Time / ns

Figure 8.

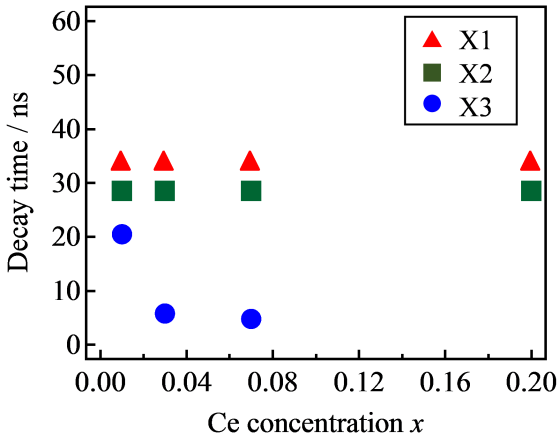
60
50
40
30
20
10
0
Decay time / ns
0.00
0.04
0.08
0.12
0.16
0.20
Ce concentration x
X1
X2
X3

Figure 9.